



## Design, Control and Performance Analysis of a Grid-Connected Hybrid System

Shazly A. Mohamed

Department of Electrical Engineering, Faculty of Engineering, South Valley University, Qena, postcode 83523, Egypt

### ARTICLE INFO

#### Article history:

Received 25 August 2017  
Received in revised form  
07 December 2017  
Accepted 15 January 2018  
Available online 25 July  
2018

#### Keywords:

PV  
Wind turbine  
Hybrid system  
DFIG  
DC-DC boost converter  
MPPT control technique

### ABSTRACT

The present paper proposes a dynamic modeling and control of grid-connected PV/Wind hybrid system. The photovoltaic and wind energy conversion systems are integrated into main AC bus in order to increase system effectiveness. The PV system is equipped with DC-DC boost converter and three phase PWM inverter. The wind energy conversion system includes doubly fed induction generator (DFIG) based variable speed wind turbine, rotor side converter (RSC) and grid side converter (GSC). The modelling, analysis and simulation of the hybrid system has been implemented using MATLAB/Simulink environment. The maximum power point tracking (MPPT) technique is applied for both photovoltaic and wind systems to capture the maximum power under varying climatic conditions. The dynamic performance of the proposed hybrid system is analyzed under different environmental conditions such as changes of solar irradiation and wind speed. The simulation results show that the voltage at point of common coupling (PCC) maintains constant. Moreover, the current of grid side is in sinusoidal and alternative form. This grid side current is synchronized with grid side voltage and injected power to grid is around power delivered by the hybrid system.

© 2018 EIEST. All rights reserved

### Nomenclature

$I_{pv}$ ,  $V_{pv}$ : Output current and voltage of PV cell.  
 $I_{ph}$ ,  $I_{sat}$ : Photocurrent and diode saturation current of PV cell.  
 $R_s$ ,  $R_{sh}$ : Series and shunt resistance of PV cell.  
 $q$ : Charge of electron ( $1.6 \times 10^{-19}$ c).  
 $A$ : P-N junction ideality factor.  
 $K$ : Boltzmann's constant ( $1.38 \times 10^{-23}$ j/k).  
 $T$ : Cell temperature [k].  
STC: Standard test condition [TSTC=25° C, GSTC=1000 W/m<sup>2</sup>].  
 $G$ : Solar irradiation.  
 $K_i$ : Short circuit current coefficient.  
 $E_g$ : Band gap energy of semiconductor.  
 $V_{in}$ : Input voltage to boost converter and output from PV system.  
 $U_{dc}$ : Output voltage from boost converter.  
 $L$ ,  $C$ : Inductance and capacitance of boost converter.  
 $d$ : Duty cycle of boost converter switch.  
 $I_o$ : Output current from boost converter.  
 $I_L$ : Input current to boost converter.  
 $\omega$ : Grid frequency.  
 $R_f$ ,  $L_f$ : Resistance and inductance of RL filter.  
 $C_{bus}$ : DC link capacitor.  
 $V_{dc}$ : DC link voltage.  
PWM: Pulse width modulation.  
PLL: Phase locked loop.  
 $\theta$ : Grid voltage angle.  
 $P_m$ : Mechanical output power of wind turbine.

$C_p$ : Performance coefficient of the wind turbine.  
 $\lambda$ ,  $\beta$ : tip speed ratio of the rotor blade and blade pitch angle.  
 $\rho$ : Air density.  
 $A$ : Turbine swept area.  
 $V_{wind}$ : Wind speed.  
 $\Phi_{ds}$ ,  $\Phi_{qs}$ : d-q stator flux components in synchronous reference frame.  
 $\Phi_{dr}$ ,  $\Phi_{qr}$ : d-q rotor flux components in synchronous reference frame.  
 $i_{ds}$ ,  $i_{qs}$ : d-q stator current components in synchronous reference frame.  
 $i_{dr}$ ,  $i_{qr}$ : d-q rotor current components in synchronous reference frame.  
 $R_s$ ,  $L_s$ : Stator resistance and stator self-inductance of DFIG.  
 $R_r$ ,  $L_r$ : Rotor resistance and rotor self-inductance of DFIG.  
 $L_m$ : Magnetizing inductance of DFIG.  
 $V_{ds}$ ,  $V_{qs}$ : d-q stator voltage components in synchronous reference frame.  
 $V_{dr}$ ,  $V_{qr}$ : d-q rotor voltage components in synchronous reference frame.  
 $\omega_e$ : Angular velocity of stator magnetizing flux.  
 $\omega_r$ : Rotational speed of rotor.  
 $\sigma$ : Leakage factor.  
 $\pm\delta$ : Fixed step size.  
 $i_{ms}$ : Stator magnetizing current.  
 $P$ : Number of pole pairs.  
 $m$ : Stator modulation factor.

## I. INTRODUCTION

Among the alternative renewable energy sources, wind and photovoltaic (PV) have attracted great attention and can be considered as the most promising technologies to produce electricity [1]. Wind power can be captured by generators with high power capacity. PV power is another promising energy source since it is global, cheap and clean both have their own demerits as they are intermittent in nature and immensely depend on the climate conditions, besides photovoltaic energy can be utilized only during daylight [2, 3]. In fact, PV and wind power are complimentary in nature since when there is no sun there is plenty of wind and vice-versa [4]. Therefore, integration of these renewable energy resources as hybrid PV/wind generation system can be used for overcoming intermittency and provide high reliability to maintain continuous output power to electrical grid or rural areas. Several control strategies have been proposed to overcome problems related to maximum power extraction and injected power quality. Over recent years several investment and research have been carried out in the hybrid PV/wind system, such as Kumar and et al. [2], who presented integration of photovoltaic (PV) and doubly-fed induction generator (DFIG) as hybrid system connected to utility grid. Adhikari and et al. [3], showed design, analysis and control of standalone hybrid renewable energy conversion system based on solar and wind energy sources. Several modeling studies on PV/DFIG power system have been conducted. Among them, Rajesh and et al. [4], investigated solar PV and doubly fed induction generator (DFIG) based wind turbine to provide sustainable power for remote areas. This study investigates detailed dynamic modeling, control and simulation of solar PV and DFIG based wind hybrid power system interconnected to electrical grid and variations in the local ac load power and dispatch power to the distribution grid are considered. The proposed system is using DC-DC boost converter with PV for MPPT and DFIG driven by variable speed wind turbine. This paper aims to study the performance analysis of grid-connected PV/wind hybrid system under different weather conditions. The rest of this paper is organized as follows after introduction: In section 2, the proposed PV/Wind hybrid system and its components are discussed. In section 3, photovoltaic conversion system is discussed. Wind conversion system and control strategy are presented in section 4. The simulation results and discussions about the performance of hybrid system are included in section 5. Finally, in section 6, summary of findings is addressed.

## 2. MODELING AND CONTROL OF THE PV/WIND HYBRID SYSTEM

Hybrid system usually consists of two or more renewable energy source to provide increased efficiency of the system and also greater balance in energy supply. The proposed configuration of the PV/Wind hybrid system is depicted in Fig. (1). It is composed of two blocks: the power block and control block. The power block consists of PV array and wind turbine as sources of energy. The PV energy conversion system is equipped with its DC-DC boost converter in order to step up array output voltage to the required voltage level (500V DC). In addition, The DC-AC inverter that converts 500V DC to 260V AC and keeps unity power factor. The wind energy conversion includes doubly fed induction generator (DFIG), rotor side converter (RSC) and grid side converter (GSC). Transformer is used in order to raise output voltage to point of common coupling (PCC) voltage. Concerning the control block, many

techniques have been investigated in order to extract maximum power, keep unity power factor and regulate DC link voltage.

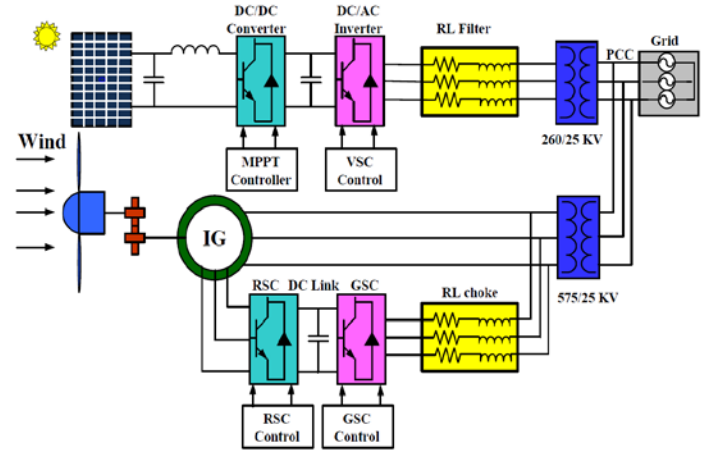


Fig. (1): The proposed model of hybrid system connected to grid

## 3. PHOTOVOLTAIC CONVERSION SYSTEM

In this section the electrical modelling of a PV module and its characteristics are introduced. In addition, the DC-DC boost converter, maximum power point tracking (MPPT) algorithm and DC-AC inverter controller are discussed.

### 3.1 PV generator model

The electrical modelling of a PV module has been introduced based on the Shockley diode as shown in Fig. (2) [5].

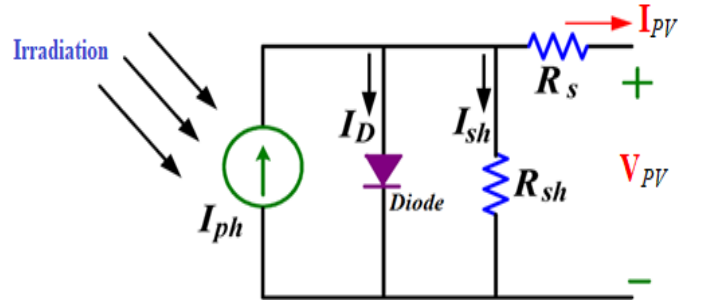


Fig. (2): Practical circuit of a PV module

The electrical characteristics of a PV module can be simulated with regard to the variations in the environmental conditions such as solar irradiation and temperature [6]. The corresponding equations that mathematically describe the (I/V) characteristics can be written as follows [7, 8]:

$$I_{PV} = I_{ph} - I_{sat} \left\{ \exp \left[ \frac{q(V_{PV} + I_{PV}R_s)}{AKT} \right] - 1 \right\} \frac{V_{PV} + I_{PV}R_s}{R_{sh}} \quad (1)$$

$$I_{ph} = \left[ I_{ph,STC} + K_i (T - T_{STC}) \right] \left( \frac{G}{G_{STC}} \right) \quad (2)$$

$$I_{sat} = I_{sat,STC} \left( \frac{T_{STC}}{T} \right)^3 \exp \left[ \frac{qE_g}{AK} \left( \frac{1}{T_{STC}} - \frac{1}{T} \right) \right] \quad (3)$$

The detailed specifications of the PV conversion system are given in Appendix. Fig. (3) depicts the (I-V) and (P-V) characteristics of PV array obtained through modelling under various solar irradiation intensity conditions.

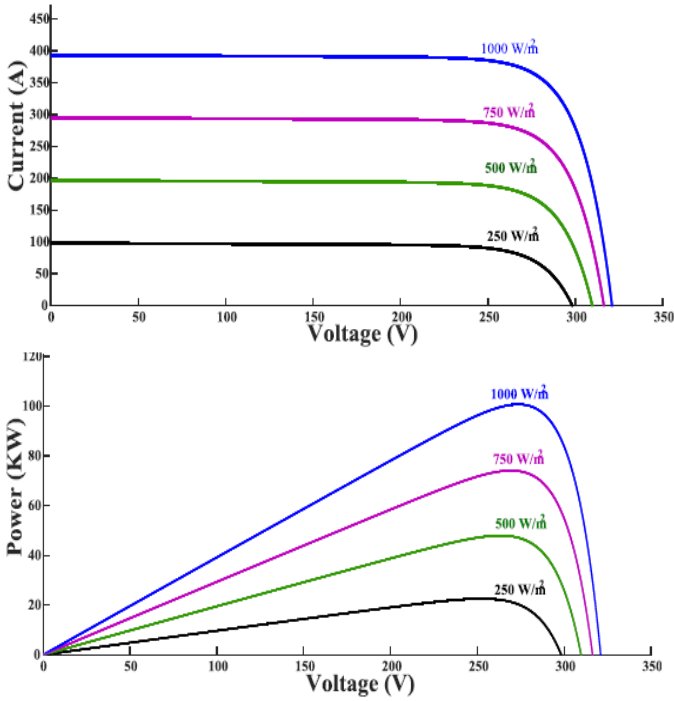


Fig. (3): Characteristics of PV array

### 3.2 DC-DC boost converter

In this research, the DC-DC boost converter was used for MPPT. Since the output voltage from PV array has a small value to be converted to AC voltage via DC-AC inverter, the boost converter steps up voltage from PV array ( $V_{MPP}=272$  VDC at irradiation of  $1000 \text{ W/m}^2$ ) to the required voltage level (500 VDC). In addition, this boost converter will present low ripple current on the PV array side [9]. The circuit depicts the connection of DC-DC boost converter to PV array is shown in Fig. (4). Switching duty cycle of boost converter is called ( $d$ ), and is piloted by MPPT controller that utilizes the "Incremental conductance + Integral regulator" technique. The boost converter in state space representation is expressed as follows [1]:

$$\begin{aligned} V_{in} &= L \frac{dI_L}{dt} + U_{dc} (1 - d) \\ C \frac{dU_{dc}}{dt} + I_o &= (1 - d)I_L \end{aligned} \quad (4)$$

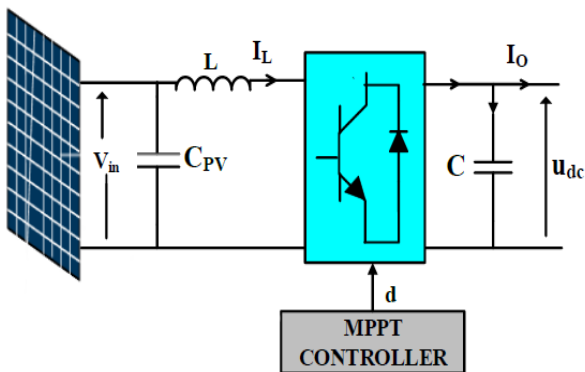


Fig. (4): Equivalent circuit of DC-DC boost converter

### 3.3 Incremental conductance (IC) technique based MPPT control algorithm

A normal PV array can convert about 40% of incident solar energy into electrical energy. Since the intensity of solar energy varies with time, maximum power point tracking or MPPT

technique is used for extracting maximum output power from PV array under certain environmental conditions [10]. Previous surveys have proposed several MPPT techniques such as fuzzy logic control, perturb and observe and particle swarm optimization [1, 7, 11]. In this study "Incremental conductance + Integral regulator" technique is used due to its simplicity and advantage of offering good performance under rapid variation of solar irradiation. The basic concept of incremental conductance MPPT technique on P-V curve is shown in Fig. (5), which the slope indicates that the derivative of power with respect to voltage is zero at the MPP, increasing on the left hand side of the MPP and decreasing on the right hand side of the MPP [12]. The mathematical model of this technique is as follows:

The output power from the PV array is:

$$P = V \times I \quad (5)$$

If the operating point is the MPP, equation (5) will be

$$\frac{dP}{dV} = 0$$

$$\frac{d}{dV} [V \times I] = I + V \frac{dI}{dV} = 0$$

Then, the following definitions are considered to track the MPP:

$$\frac{dI}{dV} = -\frac{I}{V} \quad \text{At the MPP, } \Delta V_n = 0 \quad (6)$$

$$\frac{dI}{dV} > -\frac{I}{V} \quad \text{Left of the MPP, } \Delta V_n = +\delta \quad (7)$$

$$\frac{dI}{dV} < -\frac{I}{V} \quad \text{Right of the MPP, } \Delta V_n = -\delta \quad (8)$$

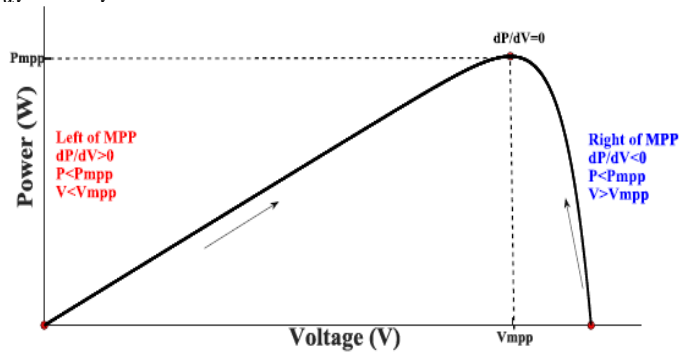


Fig. (5): Basic concept of incremental conductance MPPT technique

Fig. (6) depicts the flow chart of incremental conductance MPPT technique. In this technique the tracking of MPP is obtained by fixed step size ( $\pm\delta$ ). If the operating point is the MPP, the error signal will be zero while at the right or at the left of the MPP this error signal is applied to integral regulator switch to regulate PV output voltage.

### 3.4 DC/AC inverter controller

The proposed control scheme of DC/AC inverter is depicted in Fig. (7). A voltage oriented control (VOC) strategy is implemented to regulate the DC link voltage, control injected active power and make unity power factor. This control strategy is beneficial for its decoupled control ability and fast dynamics [13]. Then,

$$V_{abc\_inv} = V_{abc} + R_f I_{abc\_inv} + L_f \cdot \frac{dI_{abc\_inv}}{dt} \quad (9)$$

Transforming equation (9) into d-q rotating reference frame yield:

$$V_{d\_inv} = V_d + R_f I_d + L_f \frac{dI_d}{dt} - \omega L_f I_q \quad (10)$$

$$V_{q\_inv} = V_q + R_f I_q + L_f \frac{dI_q}{dt} - \omega L_f I_d \quad (11)$$

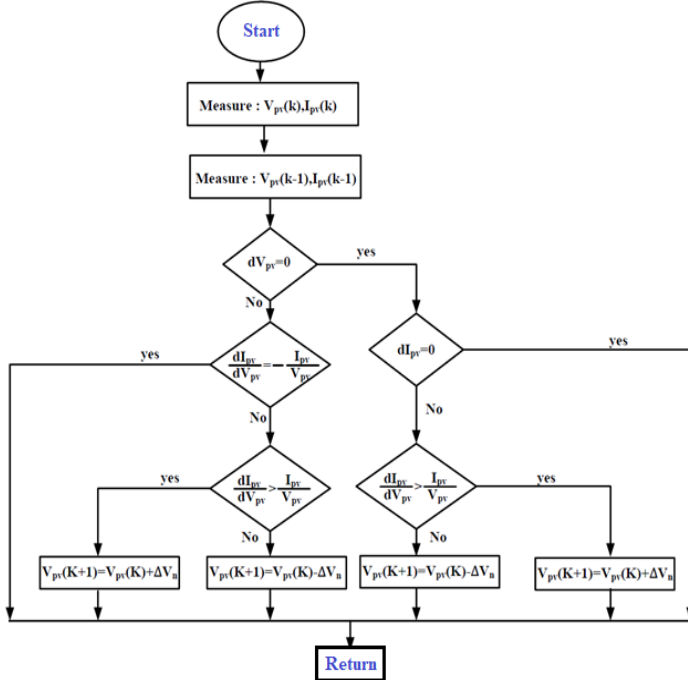


Fig. (6): Control flow chart of MPPT incremental conductance method

The Phase Locked Loop (PLL) is closed loop frequency control system. The main objective of PLL is estimation of grid voltage angle ( $\theta$ ) thus accurate synchronization between inverter output voltage and grid voltage.

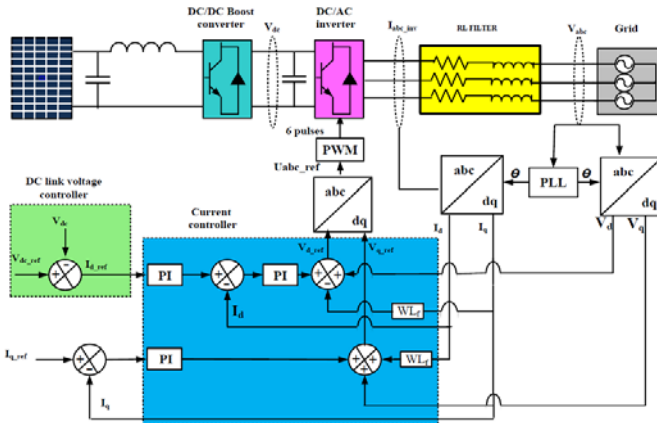


Fig. (7): Overall DC/AC inverter control scheme

### 3.4.1 DC link voltage controller

The DC link voltage control loop is responsible for regulation DC link voltage at constant specified value [14].

$$V_{dc} = 2 \cdot \sqrt{\frac{2}{3}} V_{abc\_LL,rms} \quad (12)$$

The reference DC voltage is compared with actual DC voltage and the difference is applied to PI controller to regulate DC voltage at 500 V DC. The output of this controller is used as direct axis reference current ( $I_{d-ref}$ ) for inner current controller.

### 3.4.2 Current controller

The current controller loop control independently the direct axis ( $I_d$ ) and quadrature axis ( $I_q$ ) grid currents. The ( $I_{d-ref}$ ) is derived from dc link voltage control while the ( $I_{q-ref}$ ) is imposed to zero to ensure unity power factor. Since the d-axis is aligned with vector of grid voltage, the quadrature axis grid voltage ( $V_q$ ) is imposed to zero. Thus the active and reactive power can be controlled independently by means of  $I_d$  and  $I_q$  respectively.

Then,

$$P = \frac{3}{2} (V_d I_d + V_q I_q) = \frac{3}{2} V_d I_d$$

$$Q = \frac{3}{2} V_d I_q \quad (13)$$

Output voltage  $V_{d-ref}$  and  $V_{q-ref}$  from current controller loop are converted to three different modulating signals. (Uref (a), Uref (b), Uref(c)). The three levels PWM technique utilizes these signals to generate IGBTs switching pulses.

## 4. WIND ENERGY CONVERSION SYSTEM

In this section, the mechanical modelling of wind turbine and its characteristics are discussed. In addition, doubly fed induction generator (DFIG) model, rotor side converter controller, grid side converter controller and maximum power point tracking algorithm are introduced.

### 4.1 Wind turbine model

Wind turbine is modelled by an aerodynamic input torque which drives a doubly fed induction generator (DFIG). The mechanical power ( $P_m$ ) extracted from the wind turbine is dependent on the wind velocity and is expressed as follows [15]:

$$P_m = \frac{1}{2} C_p (\lambda, \beta) A \rho (V_{wind})^3 \quad (14)$$

The performance coefficient of the wind turbine ( $C_p$ ) depends on the blade aerodynamics and represents the efficiency of the wind turbine and can be described as follows:

$$C_p (\lambda, \beta) = C_1 \left( \frac{c_2}{\lambda_i} - C_3 \beta - C_4 \right) e^{-\frac{c_5}{\lambda_i}} + C_6 \lambda \quad (15)$$

The coefficients ( $C_1$ - $C_6$ ) are given in Appendix, while  $\lambda_i$  is defined as:

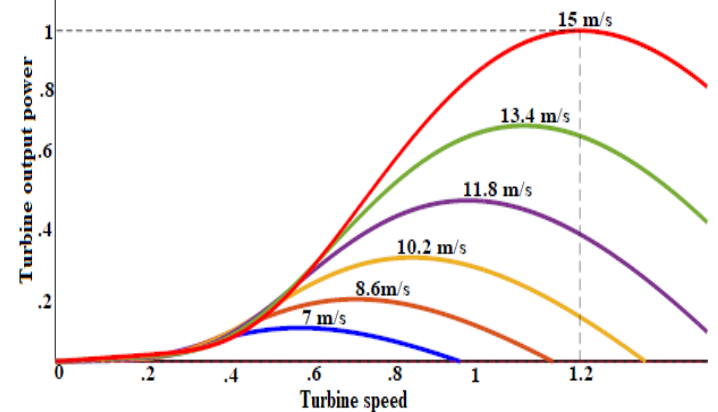
$$\frac{1}{\lambda_i} = \frac{1}{\lambda + 0.08 \beta} - \frac{0.035}{\beta^3 + 1} \quad (16)$$

Equations from (14-16) have been used in developing the mathematical model of wind turbine.

Furthermore, Equation (14) can be simplified and normalized for particular values of  $\rho$  and  $A$ , as follows:

$$P_{m-pu} = K_p C_{p-pu} V_{wind-pu}^3 \quad (17)$$

The output torque from wind turbine is transferred via drive train to the rotor of doubly fed induction generator. Fig. (8) illustrates the wind turbine power curve for different wind speeds. It is observed that the maximum power point occurs at various turbine speeds.


 Fig. (8): P-  $\omega$  curve of the wind turbine

### 4.2 Doubly Fed Induction Generator (DFIG) Model

The DFIG generates power at the stator terminals at constant voltage and at constant frequency irrespective of generator

speed. DFIG needs only to handle a fraction (25-30%) of the total power to achieve full control of generator. In the proposed control scheme, a stator flux oriented control (SFOC) is used to control separately the active and reactive power on the stator side. The stator and rotor main equations of modelling DFIG in flux linkage form can be expressed as follows [16]:

$$\begin{bmatrix} \varphi_{ds} \\ \varphi_{qs} \end{bmatrix} = L_s \begin{bmatrix} i_{ds} \\ i_{qs} \end{bmatrix} + L_m \begin{bmatrix} i_{dr} \\ i_{qr} \end{bmatrix} \quad (18)$$

$$\begin{bmatrix} \varphi_{dr} \\ \varphi_{qr} \end{bmatrix} = L_r \begin{bmatrix} i_{dr} \\ i_{qr} \end{bmatrix} + L_m \begin{bmatrix} i_{ds} \\ i_{qs} \end{bmatrix} \quad (19)$$

The mathematical modeling of DFIG in d-q synchronous reference frame for the stator and rotor voltage equations can be represented as follows [17]:

$$\begin{bmatrix} V_{ds} \\ V_{qs} \end{bmatrix} = R_s \begin{bmatrix} i_{ds} \\ i_{qs} \end{bmatrix} + (d/dt) \begin{bmatrix} \varphi_{ds} \\ \varphi_{qs} \end{bmatrix} + (\omega_e) \begin{bmatrix} -\varphi_{qs} \\ \varphi_{ds} \end{bmatrix} \quad (20)$$

$$\begin{bmatrix} V_{dr} \\ V_{qr} \end{bmatrix} = R_r \begin{bmatrix} i_{dr} \\ i_{qr} \end{bmatrix} + (d/dt) \begin{bmatrix} \varphi_{dr} \\ \varphi_{qr} \end{bmatrix} + (\omega_e - \omega_r) \begin{bmatrix} -\varphi_{qr} \\ \varphi_{dr} \end{bmatrix} \quad (21)$$

Electromagnetic torque can be expressed as follows:

$$T_e = \frac{3}{2} P \frac{L_m}{L_s} (\varphi_{ds} i_{qr} - \varphi_{qs} i_{dr}) \quad (22)$$

The active and reactive powers of the stator and rotor are computed as follows [18]:

$$P_s = \frac{3}{2} (V_{ds} i_{ds} + V_{qs} i_{qs}) \quad (23)$$

$$Q_s = \frac{3}{2} (V_{qs} i_{ds} - V_{ds} i_{qs})$$

$$P_r = \frac{3}{2} (V_{dr} i_{dr} + V_{qr} i_{qr})$$

$$Q_r = \frac{3}{2} (V_{qr} i_{dr} - V_{dr} i_{qr}) \quad (24)$$

From above equations, it is obvious that the injected power to grid can be controlled by controlling the d-q components of rotor current.

#### 4.3 Rotor Side Converter (RSC) Controllers

The main function of the RSC is to achieve maximum power point tracking (MPPT) and to control the injected reactive power by the DFIG to keep the stator at unity power factor. The stator flux oriented control (SFOC) technique has been used to obtain the controller action [19]. For stator flux orientation with stator flux  $\Phi_s$  oriented along synchronously rotating d-axis,  $\Phi_s = \Phi_{ds}$ , hence  $\Phi_{qs}=0$ . Therefore using (18)-(20), the d-q components of stator currents and voltages can be expressed as follows:

$$i_{qs} = -(L_m/L_s) i_{qr} \quad \text{And} \quad i_{ds} = (1/L_s) \varphi_{ds} - (L_m/L_s) i_{dr} \\ V_{ds} = 0.0 \quad \text{And} \quad V_{qs} = \omega_e \varphi_{ds} \quad (25)$$

The d-q components of rotor voltage references  $v_{dr}^*$  and  $v_{qr}^*$  can be expressed using (18)-(20) as follows:

$$V_{dr}^* = (V_{dr})' - (\omega_e - \omega_r) \sigma L_r i_{qr} \quad (26)$$

$$V_{qr}^* = (V_{qr})' + (\omega_e - \omega_r) ((L_m^2/L_s) i_{ms} + \sigma L_r i_{dr}) \quad (27)$$

By substituting (25) in (22) and (23), the stator active power  $P_s$ , the reactive power  $Q_s$  and the electromagnetic torque  $T_e$  can be expressed as follows [20]:

$$P_s = -\frac{3L_m}{2L_s} [\omega_e \varphi_{ds} i_{qr}^*] \quad (28)$$

$$Q_s = \frac{3}{2L_s} \left[ \frac{V_s^2}{\omega_e} - V_s L_m i_{dr}^* \right] \quad (29)$$

$$T_e^* = \frac{3}{2} P \frac{L_m}{L_s} [\varphi_{ds} i_{qr}^*] \quad (30)$$

The proposed rotor side converter control scheme is depicted in Fig. (9). The q-axis rotor voltage reference ( $v_{qr}^*$ ) can be

generated through MPPT controller after computing reference torque  $T_e^*$ . The d-axis rotor voltage reference ( $v_{dr}^*$ ) can be created from reactive power control loop. The reactive power reference ( $Q_s^*$ ) is to zero since it is considered that the needed reactive power for the DFIG can be drawn from grid side converter (GSC) and maintain the stator at unity power factor [18].

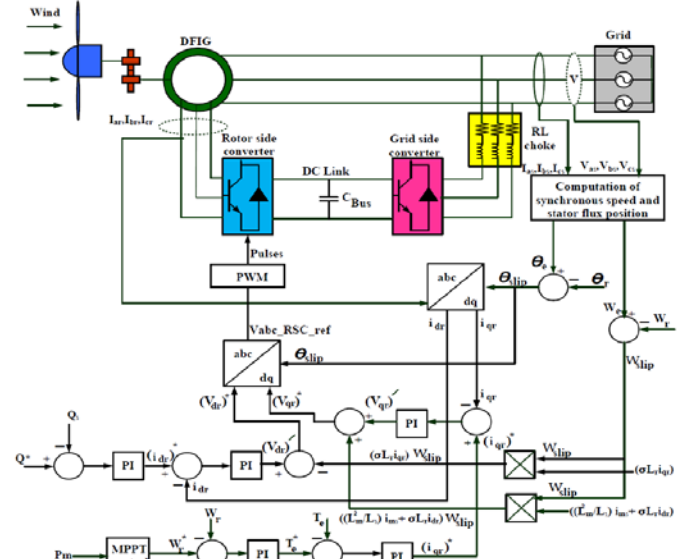


Fig. (9): Control Scheme for RSC

#### 4.4 Grid Side Converter (GSC) Controllers

The main function of the GSC is to maintain DC bus voltage constant irrespective of the magnitude and direction of power flow and to keep unity power factor at the connection point to electrical grid. The voltage for grid side converter (GSC) can be represented as follows:

$$\begin{bmatrix} V_{ag} \\ V_{bg} \\ V_{cg} \end{bmatrix} = R_{choke} \begin{bmatrix} I_{agc} \\ I_{bgc} \\ I_{cgc} \end{bmatrix} + L_{choke} \frac{d}{dt} \begin{bmatrix} I_{agc} \\ I_{bgc} \\ I_{cgc} \end{bmatrix} + \begin{bmatrix} V_{agc} \\ V_{bgc} \\ V_{cgc} \end{bmatrix} \quad (31)$$

The grid side converter voltage control equations can be transformed into d-q synchronously rotating reference frame as follows:

$$\begin{bmatrix} V_{dg} \\ V_{qg} \end{bmatrix} = R_{choke} \begin{bmatrix} i_{dgc} \\ i_{qgc} \end{bmatrix} + L \frac{d}{dt} \begin{bmatrix} i_{dgc} \\ i_{qgc} \end{bmatrix} + \omega_e L_{choke} \begin{bmatrix} -i_{qgc} \\ i_{dgc} \end{bmatrix} + \begin{bmatrix} V_{dgc} \\ V_{qgc} \end{bmatrix} \quad (32)$$

The vector control strategy with reference frame oriented along stator voltage vector position has been adopted for the controller action. Aligning the d-axis of reference frame along the grid voltage vector, then  $V_{dg}=|V_g|$ , hence  $V_{qg}=0$ . Thus using (23), the real power ( $P_g$ ) and the DC link voltage can be controlled via  $i_{dgc}^*$  while the reactive powers ( $Q_g$ ) can be controlled  $i_{qgc}^*$  as follows:

$$P_g^* = \frac{3}{2} V_{dg} i_{dgc}^* \quad (33)$$

$$Q_g^* = -\frac{3}{2} V_{dg} i_{qgc}^*$$

$$C_{bus} = \frac{dV_{dc}}{dt} = \frac{3m}{2\sqrt{2}} i_{dgc}^* - i_{or} \quad (34)$$

The proposed control structure of grid side converter (GSC) is depicted in Fig. (10). The GSC is current regulated pulse width modulation (PWM) converter, with d-axis current ( $i_{dgc}^*$ ) to regulate DC link voltage and q-axis current ( $i_{qgc}^*$ ) to regulate the exchanged reactive power with grid. The q-axis current reference ( $i_{qgc}^*$ ) is set to zero to maintain the grid at unity power

factor. The d-q reference components for the GSC voltage can be expressed as follows:

$$V_{dgc}^* = -(V_{dgc})' + (\omega_e L_{choke} i_{dgc}) + V_{dgc} \quad (35)$$

$$V_{qgc}^* = -(V_{qgc})' - (\omega_e L_{choke} i_{dgc}) \quad (36)$$

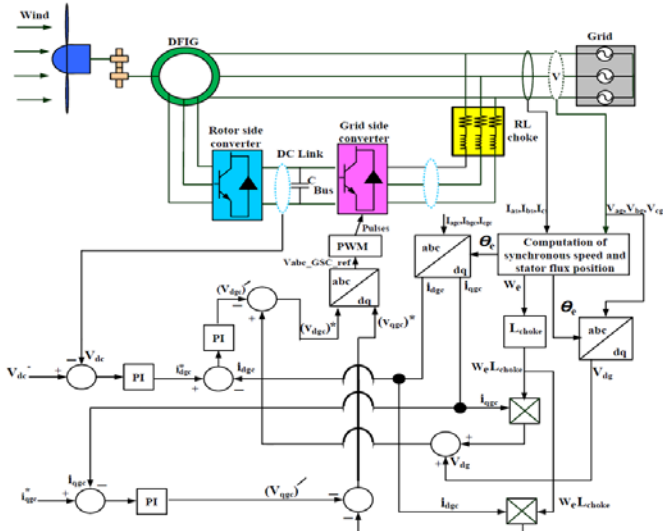


Fig. (10): Control Scheme for GSC

4.5 Adopted MPPT control strategy for WECS

The maximum power from wind turbine is extracted at optimum rotational speed of rotor ( $\omega_r^*$ ). Consequently, when wind speed varies the MPPT controller calculates this optimum rotational speed ( $\omega_r^*$ ) to track the maximum power point. Since the common MPPT techniques based on measurement of wind speed and wind turbine characteristics, the absence of accuracies in modeling of wind turbine and in wind speed measurement, will affect the precision of the MPPT controller [21]. The flow chart of the proposed MPPT controller is illustrated in Fig. (11). the proposed MPPT control technique depending on the mechanical power ( $P_{m-pu}$ ) to compute the optimum rotational speed ( $\omega_r^*$ ). The optimum rotational speed ( $\omega_r^*$ ) is normally 1.2 p.u but for mechanical power ( $P_{m-pu}$ ) levels less than 75%. The optimum rotational speed ( $\omega_r^*$ ) can be expressed as follows [22]:

$$\omega_r^* = -0.67 (P_{m-pu})^2 + 1.42 (P_{m-pu}) + 0.51 \quad (37)$$

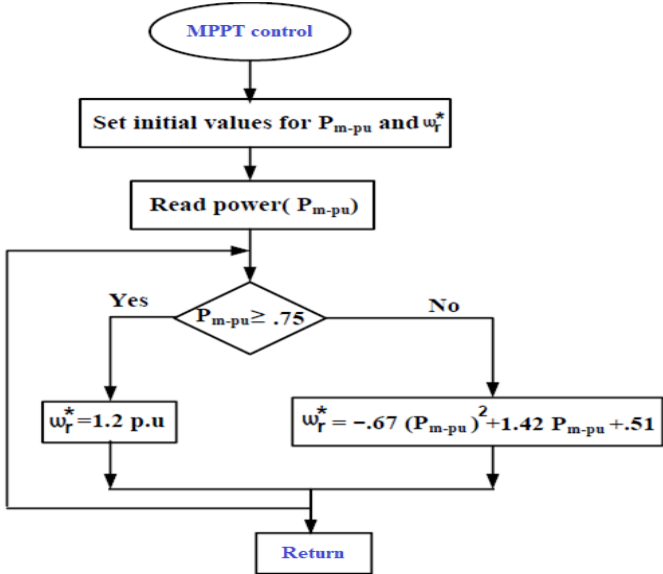


Fig. (11): Flow chart of the proposed MPPT controller

5. SIMULATION RESULTS AND DISCUSSION

The proposed model of PV/wind hybrid system shown in Fig. (1) has been simulated by using MATLAB/SIMULINK software package to verify its performance. Fig. (12) shows the overall configuration of the simulated 10-MW PV/wind hybrid system connected to grid. Detailed specifications of the proposed system are given in Appendix. The system is analyzed under different environmental conditions such as variation of solar radiation and wind speed. This section is divided into three parts: Performance of the PV conversion system, performance of wind energy conversion system and performance of PV/wind hybrid system. The simulation results show that the proposed control strategies successfully achieved the desired system performance.

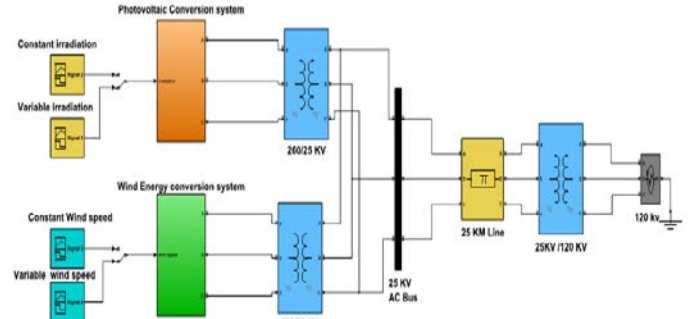


Fig. (12): Simulated model of grid-connected hybrid system

5.1 Performance of PV system

This scenario investigates the system performance under variations of solar irradiance. The PV array surface temperature is considered to be constant at 25°C during the complete simulation time. The variation of solar irradiance is depicted in Fig. (13-a).

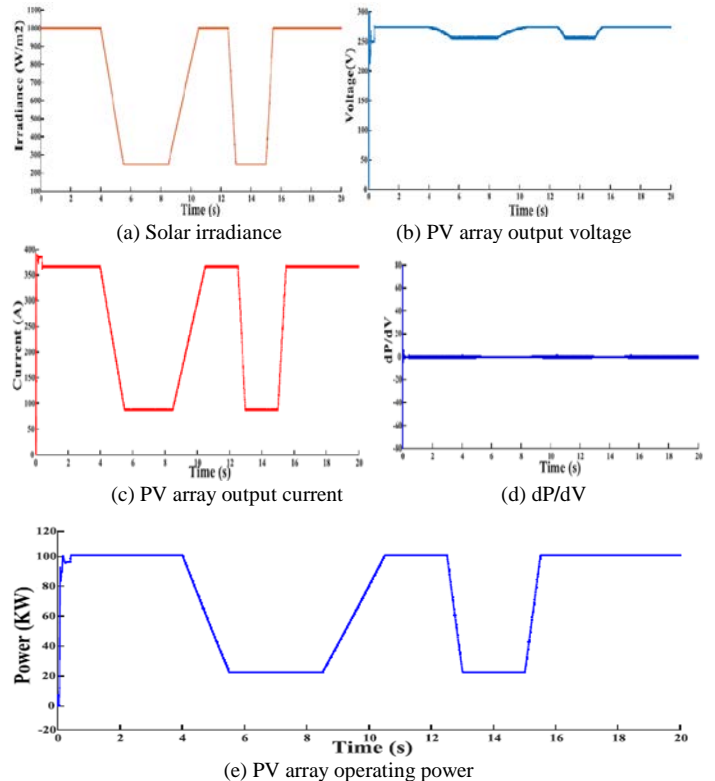


Fig. (13): Performance of PV array

PV array output voltage traces the voltage at MPP well response to variation of solar irradiance as shown in Fig. (13-b). PV array output current is influenced by solar irradiance variations as illustrated in Fig. (13-c). Since  $dP/dV$  is almost zero, the PV

array operating power points are well-tracked toward the MPPs during variations of solar irradiance as depicted in Fig. (13-d) and Fig. (13-e). Therefore the MPPT controller tracks accurately the MPPs of PV array when the solar irradiance varies continuously.

Fig. (14-a) shows the three phase injected current, it is obvious that the waveforms of three phase current are sinusoidal. It can be noticed in Fig. (14-b) that the injected active power is very near to the generated value thus small losses and the reactive power is null therefore unity power factor. In order to illustrate the proposed controller's credibility, Fig. (14-c) shows the injected voltage and current to the grid, it is clear that grid voltage and current are in phase thanks to unity power factor. Fig. (14-d) shows that the power factor of DC/AC inverter is very close to one.

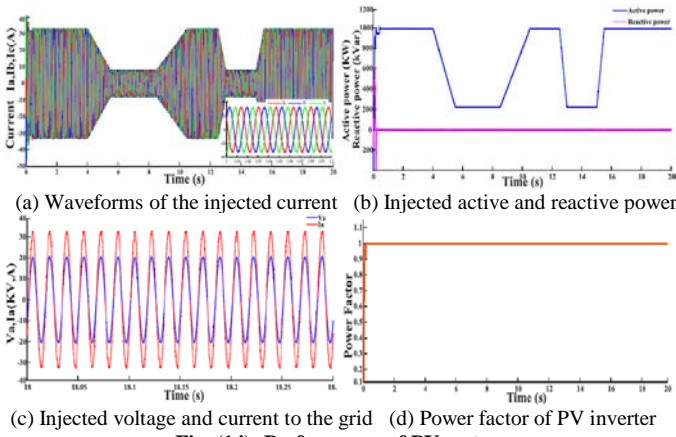


Fig. (14): Performance of PV system

5.2 Performance of wind energy system

This paper investigates the performance of wind energy conversion system under variation of wind speed. Fig. (15-a) shows the speed variation of the gradation wind. Fig. (15-b) illustrates mechanical torque of wind turbine in the process of extracting maximum wind energy. It can be noticed in Fig. (15-c) that the dc bus voltage is well kept constant at 1150V. Fig. (15-d) and Fig. (15-e) depict constant stator voltage and variation of stator current under changes of wind speed, it is clear that the waveforms of three phase stator voltage and current are sinusoidal.

Fig. (16-a) shows the injected active power from DFIG wind farm varies with wind speed while the delivered reactive power is kept zero thus unity power factor. To demonstrate the validity of grid side converter (GSC) and rotor side converter (RSC), Fig. (16-b) shows that the stator voltage and stator current are in phase thanks to zero reactive power and unity power factor. Fig. (16-c) depicts the injected current from wind energy conversion system. The change of current amplitude reflects the variation of power since grid voltage remains constant.

5.3 Performance of PV/wind hybrid system

The present paper investigates the performance of PV/wind hybrid system under variation of solar irradiation and wind speed. Fig. (17-a) shows the waveforms of three phase grid voltage, it is obvious that grid voltage remains constant. Fig. (17-b) illustrates current of grid side which is in sinusoidal and alternative form. Fig. (17-c) depicts power balance of PV/wind hybrid system, we note that the injected power from PV system is equal to 1MW under STC while the maximum power of wind energy conversion system is equal to 9 MW under base wind speed. Fig. (17-d) shows that the power delivered to grid side is

equal to sum of injected powers from PV system and wind system.

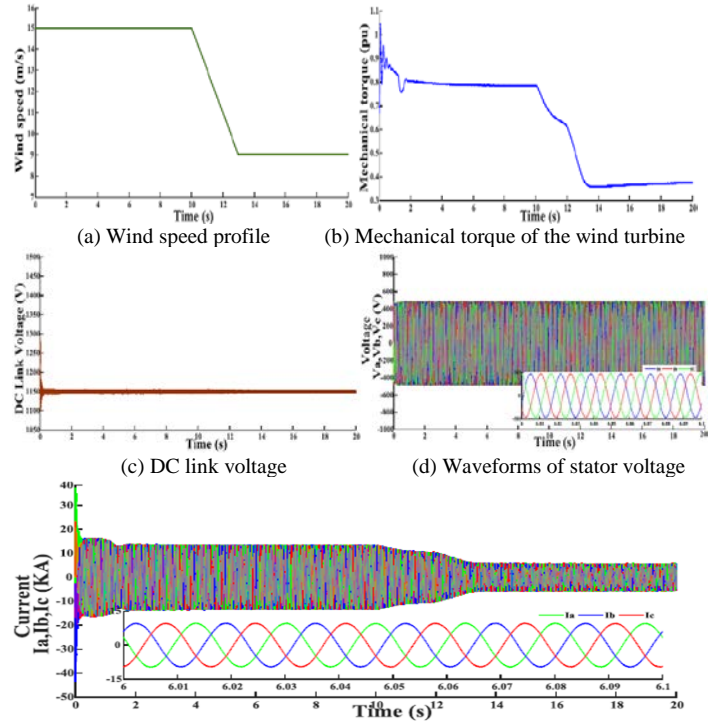


Fig. (15): Performance of DFIG

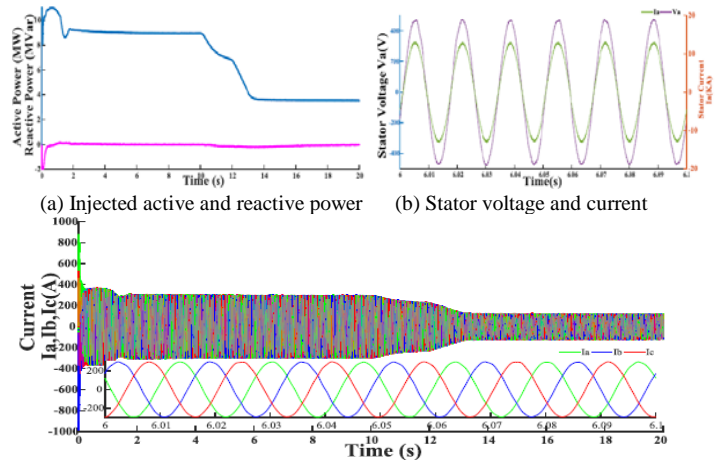


Fig. (16): Performance of wind energy system

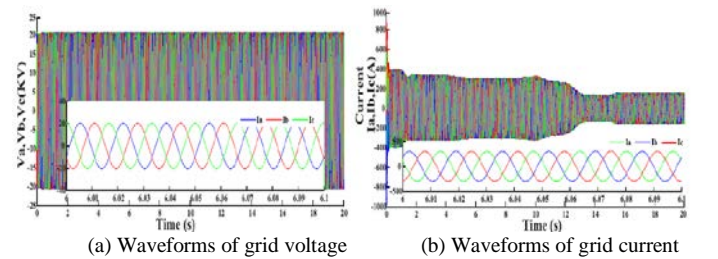


Fig. (17): Performance of PV/Wind hybrid system

6. CONCLUSION

In this research, dynamic modeling and control of grid connected photovoltaic/wind hybrid system has been successfully investigated and implemented using MATLAB/Simulink. The dynamic performance of the proposed hybrid system is tested under different environmental conditions such as variation of wind speed and solar radiation. The MPPT technique is applied to the PV system and the wind system to capture the maximum power under varying climatic conditions. The simulation results have proven the robustness of the proposed hybrid system in response to rapid changes in solar radiation and wind speed conditions.

REFERENCES

[1] M. Izadbakhsh, A. Rezvani and M. Gandomkar, "Dynamic response improvement of hybrid system by implementing ANN-GA for fast variation of photovoltaic irradiation and FLC for wind turbine", Archives of Electrical Engineering, vol. 64, pp. 291-314, 2015.

[2] M. Kumar, K. Sandhu and A. Kumar, "Simulation analysis and THD measurements of integrated PV and wind as hybrid system connected to grid", 6th IEEE International Conference on Power Electronics (IICPE), pp. 1-6, 2014.

[3] Y. Ye, Y. Fu, and S. Wei, "Simulation for grid connected wind turbines with fluctuating," Physics Procedia, vol. 24, pp. 253-260, 2012.

[4] K. Rajesh, A. Kulkarni and T. A. Padmanabha, "Modeling and Simulation of Solar PV and DFIG Based Wind Hybrid System", Procedia Technology, Vol. 21, pp. 667-675, 2015.

[5] Krismadinata, N. A. Rahim, H. W. Ping and J. Selvaraj, "Photovoltaic module modeling using Simulink/Matlab", Procedia Environmental Sciences Elsevier, Vol. 17, pp. 537-546, 2013.

[6] M. Bakkar, M. Abdel G. and M. A. zied, "Photovoltaic Maximum Power Point Grid Connected based on Power Conditioning Technique Employing Fuzzy Controller", Renewable Energy and Power Quality Journal (RE&PQJ), Vol.1, No.13, pp. 339- 344, April 2015.

[7] R. Koad, A. F. Zobia and A. El Shahat, "A Novel MPPT Algorithm Based on Particle Swarm Optimisation for Photovoltaic Systems", IEEE Transactions on Sustainable Energy, 2016.

[8] N. M. A. Shannan, N. Z. Yahaya and B. Singh, "Single-diode model and two-diode model of PV modules: A comparison", IEEE International Conference on Control System, Computing and Engineering (ICCSCE), pp. 210-214, 2013.

[9] D. S. Selvan, "Modeling and simulation of incremental conductance MPPT algorithm for photovoltaic applications", International Journal of Scientific Engineering and Technology, Volume No.2, Issue No.7, pp: 681-685, 2013.

[10] Ned Mohan, "First course on power electronics and drives", Published by MNPERE, ISBN 0-9715292-2-1, USA, 2003.

[11] T. R. Ayodele, A.-G. A. Jimoh, J. Munda, and J. Agee, "Dynamic Response of a Wind Farm Consisting of Doubly-Fed Induction Generators to Network Disturbance," in Simulation and Modeling Methodologies, Technologies and Applications, ed: Springer, pp. 131-150, 2013.

[12] S. Bae and A. Kwasinski, "Dynamic modeling and operation strategy for a microgrid with wind and photovoltaic resources", IEEE Transactions on Smart Grid, Vol. 3, pp. 1867-1876, 2012.

[13] A. Cupertino, J. De Resende, H. Pereira and S. S. Júnior, "A grid-connected photovoltaic system with a maximum power point tracker using passivity-based control applied in a boost converter", 10th IEEE/IAS International Conference on Industry Applications (INDUSCON), pp. 1-8, 2012.

[14] B. E. Strand, "Voltage Support in Distributed Generation by Power Electronics", Master of Science in Energy and Environment, January 2008.

[15] A. B. Oskouei, M. R. Banaei and M. Sabahi, "Hybrid PV/wind system with quinary asymmetric inverter without increasing DC-link number", Ain Shams Engineering Journal, Vol. 7, pp. 579-592, 2016.

[16] A. Parida and D. Chatterjee, "An improved control scheme for grid connected doubly fed induction generator considering wind-solar hybrid system", International Journal of Electrical Power & Energy Systems, Vol. 77, pp. 112-122, 2016.

[17] A. Hamadi, S. Rahmani, K. Addoweesh and K. Al-Haddad, "A modeling and control of DFIG wind and PV solar energy source generation feeding four wire isolated load", 39th Annual Conference of the IEEE Industrial Electronics Society, IECON, pp. 7778-7783, 2013.

[18] B. Singh, S. K. Aggarwal and T. C. Kandpal, "Performance of wind energy conversion system using a doubly fed induction generator for maximum power point tracking", IEEE Industry Applications Society Annual Meeting (IAS), pp. 1-7, 2010.

[19] A. Parida and D. Chatterjee, "Cogeneration topology for wind energy conversion system using doubly-fed induction generator", IET Power Electronics, Vol. 9, pp. 1406-1415, 2016.

[20] C. Subramanian, D. Casadei, A. Tani and C. Rossi, "Modeling and Simulation of Grid Connected Wind Energy Conversion System Based on a Doubly Fed Induction Generator (DFIG)", International Journal of Electrical Energy, Vol. 2, No. 2, June 2014.

[21] V. Rajasekaran, "Modeling, simulation and development of supervision control system for hybrid wind diesel system", Master of Science in Applied Science, July 19, 2013.

[22] N. W. Miller, W. W. Price and J. J. Sanchez-Gasca, "Dynamic modeling of GE 1.5 and 3.6 wind turbine-generators", GE-Power systems energy consulting, October 27, 2003.

APPENDIX

Table (1): Design parameters

Solar PV Array	
Number of arrays	10
Number of series connected modules per string	5
Number of parallel strings	96
Module type	SunPower SPR-305-WHT
Maximum power per array (PMPP)	100.7 kw
Voltage at MPP (VMPP)	273.5 V
Current at MPP (IMPP)	386.3 A
Open circuit voltage (Voc)	321 V
Short circuit current (Isc)	393.4 A
Doubly Fed Induction Generator (DFIG)	
Rotor type	Wound rotor
Rated power	6*1.5=9 MW
Stator nominal voltage (L-L)	575 V
Nominal frequency	60 Hz
Stator resistance	0.023 p.u
Stator inductance	0.18 p.u
Rotor resistance	0.016 p.u
Rotor inductance	0.16 p.u
Magnetizing inductance	2.9 p.u

Pairs of poles	3
Nominal DC link voltage	1150 V
Wind Turbine	
Base wind speed	15 m/s
Maximum power at base wind speed	1.5 MW
Base Rotational speed	1.2 p.u
Nominal performance coefficient (Cp)	0.48 p.u for $[\lambda=8.1, \beta=0]$
Aerodynamic Coefficients (c1-c6)	[0.5176,116,0.4,5,21,0.0068]
Transmission Line	
Length	25 km
Resistance/km	0.413 $\Omega$ /km
Inductance/km	0.0033 H/km
Capacitance/km	501 Pico F/km